Enhancement of CO_2 uptake and selectivity in a metal-organic framework by incorporation of thiophene functionality

Vsevolod A. Bolotov,[1] Konstantin A. Kovalenko,[1,2] Denis G. Samsonenko,[1,2] Xue Han,[3] Xinran Zhang,[3] Gemma L. Smith,[3] Laura McCormick,[4] Simon J. Teat,[4] Sihai Yang,[3] Matthew J. Lennox,[5,6] Alice Henley,[6] Elena Besley,[6] Vladimir P. Fedin,[1,2] Danil N. Dybtsev,*[1,2] and Martin Schröder,*[1,3]

[1] Nikolaev Institute of Inorganic Chemistry, Siberian Branch of the Russian Academy of Sciences, 3 Ac. Lavrentiev Ave., Novosibirsk 630090 (Russian Federation) E-mail: dan@niic.nsc.ru

[2] Novosibirsk State University, 2 Pirogova st., Novosibirsk 630090 (Russian Federation)

[3] School of Chemistry, University of Manchester, Manchester, M13 9PL (UK) E-mail: m.schroder@manchester.ac.uk

[4] Advanced Light Source, Lawrence Berkeley National Laboratory, Berkeley, California 94720 (USA)

[5] Centre for Advanced Separations Engineering, Department of Chemical Engineering, University of Bath, Bath, BA2 7AY (UK)

[6] School of Chemistry, University of Nottingham, Nottingham, NG7 2RD (UK)

Keywords: Carbon dioxide, metal-organic framework, thiophene, carboxylate, zinc, binding site, breakthrough

Abstract

The complex [$Zn_2(tdc)_2dabco$] (H_2tdc = thiophene-2,5-dicarboxylic acid; dabco = 1,4-diazabicyclooctane) shows a remarkable increase in CO_2 uptake and CO_2/N_2 selectivity compared to the non-thiophene analogue [$Zn_2(bdc)_2dabco$] (H_2bdc = benzene-1,4-dicarboxylic acid; terephthalic acid). CO_2 adsorption at 1 bar for [$Zn_2(tdc)_2dabco$] is 67.4 $cm^3 \cdot g^{-1}$ (13.2 wt.%) at 298 K and 153 $cm^3 \cdot g^{-1}$ (30.0 wt.%) at 273 K. For [$Zn_2(bdc)_2dabco$] the equivalent values are 46 $cm^3 \cdot g^{-1}$ (9.0 wt.%) and 122 $cm^3 \cdot g^{-1}$ (23.9 wt.%), respectively. The isosteric heat of adsorption for CO_2 in [$Zn_2(tdc)_2dabco$] at zero coverage is low (23.65 $kJ \cdot mol^{-1}$), ensuring facile regeneration of the porous material. The enhancement by the thiophene group on the separation of CO_2/N_2 gas mixtures has been confirmed by both ideal adsorbate solution theory (IAST) calculations and dynamic breakthrough experiments. The preferred binding sites of adsorbed CO_2 in [$Zn_2(tdc)_2dabco$] have been unambiguously determined by *in situ* single crystal diffraction studies on CO_2-loaded [$Zn_2(tdc)_2dabco$], coupled with quantum chemical calculations. These studies unveil the role of the thiophene moieties in the specific CO_2 binding *via* an induced dipole interaction between the CO_2 and the sulfur center, confirming that enhanced CO_2 capacity in [$Zn_2(tdc)_2dabco$] is achieved without the presence of open metal sites. The experimental data and the theoretical insights suggest a viable strategy for improvement of adsorption properties of already known materials through incorporation of S-based heterocycles within their porous structures.

Introduction

Carbon dioxide (CO_2) release poses one of the biggest anthropogenic impacts to the environment. While broad implementation of low-carbon fuels and strategies will reduce CO_2 release, power plants, cement and steel production represent major industries that will continue to generate exhausts which require effective purification to remove CO_2 as well as other harmful gases.[1] CO_2 sequestration through selective adsorption is viewed as one of the most promising approaches due to its simple implementation, the absence of hazardous materials, tunable selectivity and low energy costs.[2] Thus, porous materials, such as metal-organic frameworks (MOFs), with the highest CO_2 adsorption capacity at relatively low partial pressures (< 5 bar) are valuable targets for such applications.[3-10] High adsorption selectivity and high uptake under ambient conditions may be enhanced in porous materials by the incorporation of specific binding sites at the pore surface. The main strategies for the incorporation of CO_2-binding centers into MOF structures have been *via* the incorporation of basic centers such as amines functioning as Lewis bases,[11-15] and adsorption at coordinatively unsaturated metal cations as Lewis acid sites.[16-21] The former strategy is a development of the traditional approach of CO_2 capture by amines to form carbamates, and shows high uptakes and very good adsorption selectivity even under humid conditions, but also, significantly, increases the energy cost for regeneration of the adsorbate. The latter strategy employs CO_2 binding through the interaction to vacant metal sites. Despite a number of advantages such as moderate energy penalty for regeneration and tunability of the adsorption sites, such materials often only function under strictly anhydrous conditions as water competes effectively for binding at the unsaturated metal sites. Also the open metal sites usually reach saturation rapidly and thus lose their activity in selective guest binding. Since each strategy has its particular disadvantages, the development of porous materials with high adsorption selectivity, appreciable CO_2 uptake under ambient conditions, capable of working under humid environments and possessing a low regeneration penalty requires new approaches based on other types of inter- and supra-molecular interactions. With a handful of exceptions,[19,22-27] weak van der Waals and supramolecular interactions have not been widely considered as a driving force for specific CO_2 binding which could result in appreciable adsorption selectivity and improved storage capacity. We demonstrate herein that the incorporation of thiophene moieties with polarizable sulfur heteroatoms, capable of induced dipole-dipole interactions, results in a remarkable increase of the CO_2 binding affinity of the microporous MOF, $[Zn_2(tdc)_2dabco]$. This increases both the storage capacity and selectivity of the framework at ambient conditions by as much as 50%,

comparing thiophene with phenyl functionalization, and also maintains the heat of adsorption at a low level to minimize penalty costs for regeneration. The enhanced CO_2 binding property of the thiophene-containing MOF has also been confirmed by fixed-bed breakthrough separation of a CO_2/N_2 mixture. More importantly, adsorbed CO_2 molecules within $[Zn_2(tdc)_2dabco]$ have been directly observed and quantified by *in situ* single crystal diffraction experiments, revealing the preferential host-guest binding interaction in the pores. The mechanism of MOF-CO_2 binding has also been studied by quantum chemical calculations, giving detailed insights on the role of the sulfur atoms in the CO_2 supramolecular binding. These results provide a new viable strategy underpinning the development of MOF materials with improved uptake and selectivity for CO_2.

Materials and Methods

All chemicals were of analytical grade and were used without additional purification. DMF was dried over the activated molecular sieves (3Å) prior to use.

Synthesis of $[Zn_2(tdc)_2dabco]\cdot 4DMF$ (**1**). To a mixture of $Zn(NO_3)_2\cdot 6H_2O$ (120 mg, 404 μmol) and thiophene-2,5-dicarboxylic acid (H_2tdc) (47 mg, 273 μmol) in DMF (5.3 ml) was added dabco (23 mg, 205 μmol) in DMF (4.0 ml) dropwise under rigorous stirring to avoid the formation of any precipitate. The resulting clear solution was heated at 100 °C for 20 h. The colorless block-shaped crystals were collected and washed with DMF. Yield: 0.093 mg (78% based on H_2tdc). Elemental analyses. Calculated for $[Zn_2(tdc)_2dabco]\cdot 4DMF\cdot H_2O$: C, 40.3; H, 5.2; N, 9.4; S, 7.2. Found: C, 40.4; H, 5.0; N, 9.2; S, 7.4. Thermogravimetric analysis. Calculated for 4DMF: 33.4%. Found: 30.5%. FT-IR (KBr): 1667 cm^{-1} (νC=O of DMF).

Synthesis of $[Zn_2(tdc)_2bpe]\cdot 2DMF$ (**2**) and **$[Zn_2(tdc)_2bpp]\cdot 2DMF$** (**3**) was carried out using a similar procedure starting from $Zn(NO_2)_2\cdot 6H_2O$ (250 mg, 842 μmol), H_2tdc (145mg, 843 μmol) and either 1,2-bis(4-pyridyl)ethane (bpe) (75mg, 408 μmol) or 1,3-bis(4-pyridyl)propane (bpp) (84mg, 424 μmol). The corresponding solids were dissolved in DMF (10 ml) with rigorous stirring and sonification. An unknown precipitate was removed from the reaction solution by centrifugation and the clear solution heated at 100 °C for 40 h. Block-shaped crystals of the product were collected and washed in DMF. The yields are 236 mg (69%) for **2** and 263 mg (73%) for **3**. Elemental analyses. Calculated for $[Zn_2(tdc)_2bpe]\cdot 2DMF$: C, 45.0; H,

3.8; N, 7.0; S, 8.0. Found: C, 45.0; H, 3.9; N, 7.0; S, 7.8. Calculated for $[Zn_2(tdc)_2bpp]\cdot 2DMF$: C, 45.7; H, 4.0; N, 6.9; S, 7.9. Found: C, 45.3; H, 3.9; N, 6.8; S, 7.5. Thermogravimetric analysis for **2**. Calculated for 2DMF: 18.3%. Found: 17.8%. Thermogravimetric analysis for **3**. Calculated for 2DMF: 18.0%. Found: 17.4%. FT-IR (KBr): **2**, 1675 cm^{-1}; **3**, 1666 cm^{-1} (νC=O of DMF).

Synthesis of activated $[Zn_2(tdc)_2dabco]$ (**1a**). The as-synthesized compound **1** was heated at 90 °C in *vacuo* for 10 h. The sample weight loss was 30.3%. Elemental analyses. Calculated for $[Zn_2(tdc)_2dabco]\cdot H_2O$: C, 36.0; H, 3.0; N, 4.7; S, 10.7. Found: C, 36.2; H, 3.0; N, 4.8; S, 10.9.

Synthesis of $[Zn_2(tdc)_2bpe]$ (**2**) and **$[Zn_2(tdc)_2bpp]$** (**3**): The as-synthesized crystals of **2** or **3** were heated at 100 °C in *vacuo* for 6 h. The sample weight loss was found to be 18.4% for **2** and 17.7% for **3**. Elemental analyses. Calculated for $[Zn_2(tdc)_2bpe]$: C, 44.0; H, 2.5; N, 4.3; S, 9.8. Found: C, 43.7; H, 2.4; N, 4.2; S, 9.5. Calculated for $[Zn_2(tdc)_2bpp]\cdot \frac{2}{3}H_2O$: C, 44.1; H, 2.9; N, 4.1; S, 9.4. Found: C, 44.5; H, 2.7; N, 4.2; S, 9.0.

Results and discussion

Synthesis and crystal structure analysis

The coordination polymer $[Zn_2(tdc)_2dabco]\cdot 4DMF$ (**1**) was prepared by solvothermal reaction of $Zn(NO_3)_2$, thiophene-2,5-dicarboxylic acid (H_2tdc) and dabco in hot DMF (100 °C) to give rectangular colorless stick-like single crystals, which were analyzed by single crystal X-ray diffraction. **1** crystallizes in tetragonal space group $P\bar{4}2_1c$ and incorporates binuclear paddle-wheel nodes $[Zn_2(OOCR)_4]$ (Fig. 1a) bound by four carboxylate groups of tdc^{2-} anions to form a slightly squeezed layer of square-grid topology with a corrugated overall structure (Fig. 1b). The remaining available coordination site at the square pyramidal Zn(II) cations are bound by N-donors of the dabco ligands, which connect $[Zn_2(tdc)_2]$ layers into a 3D porous framework with a scaffold-like primitive cubic topology **pcu** (Fig. 1c). The rotation of the dabco ligands results, as expected, in severe disorder of the carbon atoms of the CH_2CH_2 moieties, and the rigid angular shape of the tdc^{2-} anion forces notable distortions of the paddle-wheel unit such that the Zn-Zn axis is twisted from the *c* crystallographic direction of the unit cell by *ca*. 16°. The aperture of the channels running along the 4-fold axis is 5×8 Å corresponding to the shape of the squeezed square window of the $[Zn_2(tdc)_2]$ layer (Fig. 1d). These corrugated layers stack along the *c* direction in an alternating ABAB fashion, forming two different types of smaller windows across the 4-fold axis. The narrower window has dimensions of 2.5×5 Å

formed by two closely located tdc^{2-} moieties. The wider 3.5×5 Å window is formed by two tdc^{2-} arcs bent outwards from each other with an interatomic S···S distance of 8.5 Å (Fig. 1e). It is worth noting that the slight tilting of the thiophene groups [*i.e.*, the orientation of the heteroatom (*vide supra*)] results in two different types of pore environment (Fig. 3b). Regardless of this tilting, both types of channels have similar aperture and are set up for diffusion of gas molecules with potential interaction with the sulfur atoms of the thiophene moieties.

In a similar manner, two additional microporous zinc(II) thiophene-2,5-dicarboxylates $[Zn_2(tdc)_2bpe]\cdot 2DMF$ (**2**) and $[Zn_2(tdc)_2bpp]\cdot 2DMF$ (**3**) were synthesized using 1,2-bis(4-pyridyl)ethane (bpe) and 1,3-bis(4-pyridyl)propane (bpp) as N-donor bridging ligands, respectively. During the course of this work the synthesis and structure of **2** has been reported.[28] In **2** and **3** the structure of the $[Zn_2(tdc)_2]$ corrugated layer remains unchanged compared to **1**, and these layers are connected through longer N-donor linkers (Fig. 2). The elongation of the bridging ligand does open up the possibility for framework interpenetration, which is not possible for **1** incorporating shorter dabco ligands.[29] As a result the structure **1** is a single non-interpenetrated net, while **2** and **3** show doubly-interwoven structures with **pcu** topology. Despite the interpenetration, both **2** and **3** contain microporous volume filled with solvent molecules in the as-synthesized materials. We should also note that in spite of our numerous attempts to obtain similar structures with 4,4′-bipyridyl or *trans*-bis(4-pyridyl)ethylene bridging ligands we could not crystallize any product thus far. The problem could be related to steric constraint of substantially skewed $[Zn_2(OOCR)_4]$ paddle-wheel building units, which cannot be inter-connected by structurally rigid linear ligands. Dabco is an apparent exception due to its aliphatic nature and the formation of rather strong metal-ligand coordination bonds. The micropores of the as-synthesized materials **1-3** are filled by DMF solvent molecules which were located from the X-ray diffraction data. The FT-IR spectra and the chemical and thermogravimetric analyses confirm the nature and composition of the guest molecules. According to TGA data the DMF molecules can be removed by heating the material to 170–190 °C, while the irreversible thermolysis of the metal-organic framework takes place near 300 °C for **1** and **2**, or 330 °C for **3**.

The guest-free sample $[Zn_2(tdc)_2dabco]$ (**1a**) was obtained by thermal activation of the as-synthesized crystals **1** in *vacuo*. The crystalline material was sufficiently robust to sustain the activation procedure so we were able to characterize the solvent-free open structure **1a** by single-crystal X-ray

diffraction. The space group was found to be *I*4/*mmm* (tetragonal) and the local coordination of the metal cations as well as the overall **pcu** connectivity remains unchanged from **1** (Fig. 3a). The only notable difference is that the anionic tdc^{2-} linkers are more linear in the guest-free structure **1a**, resulting in a higher symmetry and a more regular structure with rectangular channels of aperture 6.5 × 6.5 Å (Fig. 3b). This straightening of the organic ligands results in an overall expansion of the guest-free structure **1a**, compared to the solvated material **1**. The total unit cell volume increases during the activation by *ca*. 3%. Notably, the structural changes between **1** and **1a** are fully reversible as the guest free compound **1a** shrinks back when placed in DMF solvent to re-form **1**. It is worth noting that the analogous compound based on terephthalate bdc^{2-} bridging ligands $[Zn_2(bdc)_2dabco]\cdot x(solv)$ (**4**) features the same reversible structural changes upon the framework activation and re-solvation, though the degree of volume expansion/contraction of the unit cell in **4** is somewhat greater (3–5%) depending on the nature of the solvent.[30,31]

Gas adsorption studies

Activation of the interpenetrated compounds **2** and **3** was achieved by heating the compounds *in vacuo* at 100 °C for 6 h. The complete removal of the guest DMF molecules without framework collapse was confirmed by powder X-ray diffraction (PXRD), TGA, chemical analyses and IR spectroscopy. Some shift of the PXRD peaks to higher 2θ angles upon de-solvation of **3** indicates a shrinkage of the partially flexible framework. N_2 adsorption measurements for the activated samples at 77 K showed reversible type I isotherms, characteristic of microporous materials, with pore volumes of 0.19 and 0.20 $cm^3\cdot g^{-1}$ and BET surface areas of 447 and 407 $m^2\cdot g^{-1}$ for **2** and **3**, respectively (See ESI). The relatively low porosity for these compounds is not surprising given the observed two-fold interpenetrated structures for these species.

The stability and permanent porosity of the guest free compound **1a** was confirmed by PXRD and gas adsorption measurements. The N_2 isotherm at 77 K reveals a type I reversible isotherm (Fig. 4) with a pore volume of 0.68 $cm^3\cdot g^{-1}$ and BET surface area of 1553 $m^2\cdot g^{-1}$. The pore volume is similar to the expected value of 0.63 $cm^3\cdot g^{-1}$ calculated from the gravimetric density of the framework **1a** (0.94 $g\cdot cm^{-3}$) and its guest accessible volume (0.59 v/v) according to the PLATON SOLV routine.[32] This is entirely consistent with the complete activation of the material and the overall stability of the porous structure under these conditions. The pore-size distribution, calculated from the N_2 isotherm, gives a sharp peak near 8 Å,

which corresponds to the diameter of the cubic cages in **1a** (*ca*. 8–9 Å). The pore volume of **1a** and its specific surface area are very close to those reported earlier for the terephthalate analogue [$Zn_2(bdc)_2dabco$] (**4a**) (0.75 $cm^3 \cdot g^{-1}$ and 1450 $m^2 \cdot g^{-1}$, respectively).[33] Consistent with these surface area data, the H_2 adsorption for **1a** (245 $cm^3 \cdot g^{-1}$ and 2.23 wt.% at 77K and 1 bar) is slightly higher than for **4a** (2.0 wt.%) under similar conditions.

The reported CO_2 adsorption measurements for **4a**,[34,35] as well as our data (see ESI) indicate rather moderate gas uptake of 9.0 wt.% (46 $cm^3 \cdot g^{-1}$) at 298K and 1 bar, and 23.9 wt.% (122 $cm^3 \cdot g^{-1}$) at 273 K and 1 bar. In contrast, CO_2 adsorption in **1a**, which generally shows similar porosity as **4a**, reveals a significant increase of *ca* 50% in uptake under the same conditions. The maximum CO_2 adsorption in **1a** at 1 bar reaches as high as 13.2 wt% (67.4 $cm^3 \cdot g^{-1}$) at 298 K and 1 bar, and 30.0 wt% (153 $cm^3 \cdot g^{-1}$) at 273 K and 1 bar (Fig. 5). At a pressure of 0.15 bar, which is relevant to the flue gas processing, the CO_2 uptakes of **1a** are 18.5 wt.% and 8.5 wt.% at 273 and 298 K, respectively. Thus, the thiophene-based **1** demonstrates excellent CO_2 adsorption properties, outperforming the majority of known porous MOFs, including those with open metal sites.[5-7]

The isosteric heat of adsorption for CO_2 in **4a** at zero coverage, calculated from the isotherms at 273 and 298 K using the Clausius-Clapeyron equation is 19.52 $kJ \cdot mol^{-1}$ consistent with literature data.[36] The heat of the adsorption of CO_2 for **1a** is noticeably higher at 23.65 $kJ \cdot mol^{-1}$, reflecting presumably stronger binding of CO_2 to the thiophene ring. The modest adsorption enthalpy of **1a** highlights the absence of the strong binding centers in **1a** with open metal sites and active amines reported to increase the heat of adsorption to 35–45 $kJ \cdot mol^{-1}$ and 50–100 $kJ \cdot mol^{-1}$, respectively.[5,6] Despite the negative impact to the selectivity,[37] the low heat of the adsorption in **1a** decreases the energy penalty for the regeneration of the porous material in a temperature-swing process.

Gas adsorption selectivity and gas separation studies

Together with the CO_2 uptake, the CO_2/N_2 adsorption selectivity is one of the most important parameters for the practical application of porous materials in the purification of the industrial exhausts.[38] The adsorption data (see ESI) allowed us to calculate the CO_2/N_2 selectivity factors for **1a** and **4a** at 298 K by three commonly used methodologies *via* i. the ratio of the adsorbed gas volume, ii. the ratio of the Henry's

constants, and iii. using ideal adsorbed solution theory (IAST). The selectivity, calculated as the ratio of the adsorbed gas volumes by **1a** at 1 bar, is $V(CO_2)/V(N_2)$ = 15.1 (Fig. 5). By considering a typical flue gas composition of 0.15 bar CO_2 and 0.75 bar N_2, the normalized[37] selectivity of adsorption at this composition can be calculated S_{ads} = 11.4. The corresponding numbers for **4a** are $V(CO_2)/V(N_2)$ = 10.2 and S_{ads} = 9.4. The Henry's constants (K_H) were derived from the linear approximation of the low pressure part of the isotherms, and based on the obtained values of K_H for **1a** and 4**a**, and the selectivity factors at 298 K were calculated to be 12.5 and 8.9, respectively. The IAST[39] calculations for **1a** resulted in a selectivity factor of 11.2 for an equimolar CO_2/N_2 mixture, while for **4a** this factor is 9.2. Thus, comparison of the above selectivity factors for **1a** and **4a** concludes that substitution of a phenyl group to thiophene on going from **4a** to **1a** enhances the CO_2/N_2 adsorption selectivity by 20 to 50%, depending upon the methodology used. Finally, it is important to note that even though the obtained selectivity factors for **1a** are lower than those for MOFs with strong CO_2 binding centers, a selectivity above 8 is high enough to be considered for practical applications.[40]

The potential of utilising these MOFs for CO_2 separation has also been confirmed in breakthrough experiments in which an equimolar mixture of CO_2/N_2 was flowed over a packed bed of **1a** at 298 K and 1.0 bar (Fig. 6). To validate the role of thiophene group in enhanced CO_2 binding, corresponding breakthrough experiment has also been conducted on the phenyl-functionalized material **4a** under the same conditions. As predicted by the selectivity calculations, a complete separation has been achieved in both cases, with N_2 being the first to elute through the bed, whereas CO_2 was retained. On saturation, CO_2 breaks through from the bed and reaches saturation rapidly. As shown in Fig. 6, dimensionless breakthrough plots offer a direct comparison between **1a** and **4a** on the performance of separation of the CO_2/N_2 mixture. Significantly, **1a** shows a pronouncedly better separation than **4a** ($\Delta\tau$ = 130 and 87 for **1a** and **4a**, respectively). Additionally, the enhanced CO_2 storage capacity by the thiophene functionalization in **1a** has been confirmed by its notably delayed (almost a factor of 2) breakthrough of CO_2 (τ = 250 and 143 for **1a** and **4a**, respectively). These results confirm the potential application of 1a on CO_2/N_2 separation.

Theoretical studies

Achieving such an outstanding affinity towards CO_2 in the absence of strong Lewis basic centers or coordinatively unsaturated metal sites prompted us to thoroughly investigate the nature of the CO_2 binding in **1a**. The main difference between **1a** and **4a** is the chemical environment of the microporous surface as the

channels in **1a** are decorated by sulfur atoms from the thiophene-2,5-dicarboxylate linkers. In the absence of any stronger intermolecular interactions (such as donor-acceptor bonds or H-bonds) the CO_2 guest molecules have to interact with the porous host through somewhat weaker dipole-dipole interactions. The sulfur atom is more susceptible to polarization and thus for the induced dipole interactions with the quadrupole of CO_2. Comparison of $[Zr_6O_4(OH)_4(bpdc)_6]$ with $[Zr_6O_4(OH)_4(btdc)_6]$ ($bpdc^{2-}$ = biphenyl-4,4'-dicarboxylate, $btdc^{2-}$ = bithiophenedicarboxylate) shows, depending on the temperature, a 32 to 78% increase for the gravimetric CO_2 uptake for the latter thiophene-containing structure.[25] It was suggested that differences in the electrostatic surface potentials for $bpdc^{2-}$ and $btdc^{2-}$ accounted for this difference, but no direct chemical explanation was given. In order to understand the role of the tdc^{2-} ligand in CO_2 adsorption in **1a**, we undertook grand canonical Monte Carlo (GCMC) simulations (see ESI). These reveal unambiguously that CO_2 is preferentially adsorbed near the tdc^{2-} linker at low loading (Fig. 7a) and that thiophene plays a key role in the adsorption of CO_2 at low pressure. The $CO_2\cdots tdc^{2-}$ interaction was probed further by DFT simulations, which confirmed that the carbon-sulfur bond provides an excellent binding site for CO_2 (Fig. 7b,c), with calculated binding energies ranging from –15.7 to –18.3 $kJ\cdot mol^{-1}$, *ca.* 3-10 $kJ\cdot mol^{-1}$ stronger than reported binding energies for CO_2 with benzene-based moieties.[41-43] The shortest S···C interatomic distance in the energy-optimized thiophene···CO_2 complex is 3.51 Å (Fig. 7c), equal to the sum of the van-der-Waals radii of sulfur and carbon. The simulated heat of CO_2 adsorption in **1a** (24.2 $kJ\cdot mol^{-1}$) coincides with the experimental value (23.65 $kJ\cdot mol^{-1}$), giving consistency between the theory and the experiment. The lower value of heat of adsorption of CO_2 for **4a** (19.6 $kJ\cdot mol^{-1}$),[33] calculated by DFT, suggests and generalizes the idea that the inclusion of thiophene-based ligands in MOFs provides a route to materials with an increased affinities for CO_2.

Determination of the binding cites for adsorbed CO_2

We also sought to determine the preferred binding sites of adsorbed CO_2 molecules in the extended pore structure of **1a** by *in situ* synchrotron X-ray single-crystal diffraction. Desolvated sample of **1a** shows complete retention of the framework structure and removal of the free guest solvent molecules from the pore (Fig. 8a). Two types of pores can be clearly observed and are denoted as α and β with a pore diameter of 7.1 Å and 7.8 Å (taking into consideration of van der Waal radii), respectively. The S centers of all thiophene

groups point into pore α, whereas pore β is primarily functionalized with –CH moieties on the thiophene. The desolvated **1a** was then loaded with CO_2 at a pressure of 1.0 bar at 273 K and diffraction data collected at time *t* = 0.25, 1, and 2 hours to capture the dynamic information of site population. It is worth mentioning that the kinetics of gas uptake in single crystals could be notably different to that of powder sample typically used in isotherm experiments. Analysis of the diffraction data indicates an absence of notable structural phase change of **1a** upon CO_2 inclusion. Sequential Fourier difference map analysis of the diffraction data revealed the position of the adsorbed CO_2 molecules in all three structures (Fig. 8 b–d).

At the first dataset of CO_2-loaded **1a**, only one binding site, (CO_2^I) was located within the pore α of **1a**·$(CO_2)_{0.40}$. CO_2^I (occupancy = 0.20) is located near the {Zn_2} paddle-wheel stabilised by dipole interactions to the paddle-wheel and hydrogen bonds to the –CH groups (Fig. S6). Upon the second data collection, **1a**·$(CO_2)_{1.56}$, the occupancy of CO_2^I increases to 0.43, accompanied by the appearance of a second binding site (CO_2^{II}) with an occupancy of 0.352. CO_2^{II} was located in pore β and is close to the thiophene group (Fig. S7). Interestingly, the CO_2–thiophene interatomic distance found in the X-ray diffraction data (3.49 Å) is highly consistent with that (3.51 Å) obtained in the DFT calculation. On additional equilibrium time (t = 2h), **1a**·$(CO_2)_{1.63}$, the occupancies of CO_2^I and CO_2^{II} drop slightly to 0.38 and 0.29, respectively, indicating a re-distribution of adsorbed CO_2 molecules. The rest of adsorbed CO_2 molecules fill into a third site (CO_2^{III}) with an occupancy of 0.14 (Fig. S8). CO_2^{III} was found in pore α, forming intermolecular dipole interaction with CO_2^I in a "T-shape" manner. Additional diffraction data collection at t > 2h yielded same crystal structures as **1a**·$(CO_2)_{1.63}$, indicating the presence of adsorption equilibrium. Thus, two out of the three CO_2 binding sites are found within the sulfur-rich pore α of **1a**, confirming the critical role of this heteroatom functionalization in carbon dioxide adsorption. Indeed, the observation of direct host-guest interaction between the thiophene and CO_2^{II} represents the first experimental evidence of CO_2 binding to a sulfur-rich functional group in MOFs.

Conclusions

Three isoreticular porous MOFs based on [$Zn_2(OOCR)_4$] paddle-wheels, connected through thiophene-2,5-dicarboxylate moieties and N-donor linkers (L) [$Zn_2(tdc)_2L$] have been synthesized and characterized. Apart from some structural distortions these frameworks are very similar to the prototypic Zn(II) terephthalate material [$Zn_2(bdc)_2$dabco] and has similar porosity in terms of pore size, volume and specific surface area.

However, substitution of a phenyl group with thiophene substantially increases adsorption of CO_2 as well as CO_2/N_2 separation selectivity as evidenced by thorough gas isotherm measurements and breakthrough experiments. The thiophene-lined $[Zn_2(tdc)_2dabco]$ possesses a very good CO_2 uptake under ambient condition even though it features neither basic amine functions nor open metal sites, which is reflected by a low isosteric heat of adsorption. The *in situ* synchrotron X-ray diffraction data and quantum chemical calculation confirm the role of the thiophene heterocycle and, particularly, sulfur atoms in binding CO_2 *via* induced dipole interactions. These results emphasize the feasibility of van der Waals interactions to effective CO_2 binding while maintaining low heat of adsorption within a hydrophobic porous material. More importantly, the incorporation of heterocycles into porous structures may represent a viable route to improving the adsorption properties of already known materials.

ASSOCIATED CONTENT

Supplementary information available: the details of the analytical methods, X-ray single crystal experiments, CIF files, gas adsorption measurements, GCMC and DFT calculation, additional figures and plots. CCDC 1503063-1503066 and 1568882-1568885 contain the supplementary crystallographic data for this paper. These data can be obtained free of charge from the Cambridge Crystallographic Data Center at http://www.ccdc.cam.ac.uk/data_request/cif.

AUTHOR INFORMATION

Corresponding Authors

dan@niic.nsc.ru; M.Schroder@manchester.ac.uk

Competing financial interests

The authors declare no competing financial interests.

Acknowledgements

We thank EPSRC, ERC and University of Manchester for funding. NIIC team is grateful to the Russian Science Foundation (Grant 14-23-00013) for the financial support. We thank the University of Nottingham for HPC facilities. M.S. acknowledges the Russian Ministry of Science and Education for the award of a

Russian Megagrant (14.Z50.31.0006). We are especially grateful to the Advanced Light Source for access to Beamline 11.3.1. The Advanced Light Source is supported by the Director, Office of Science, Office of Basic Energy Sciences, of the U.S. Department of Energy under Contract No. DE-AC02-05CH11231. The development of the gas cell used in this work was partially funded by the Center for Gas Separations Relevant to Clean Energy Technologies, an Energy Frontier Research Center funded by the U.S. Department of Energy, Office of Science, Basic Energy Sciences under Award # DE-SC0001015.

References

(1) Yuan, Z.; Eden, M. R.; Gani, R. Toward the Development and Deployment of Large-Scale Carbon Dioxide Capture and Conversion Processes. *Ind. Eng. Chem. Res.* **2016**, *55*, 3383–3419.

(2) Huck, J. M.; Lin, L.-C.; Berger, A. H.; Niknam Shahrak, M.; Martin, R. L.; Bhown, A. S.; Haranczyk, M.; Reuter, K.; Smit, B. Evaluating different classes of porous materials for carbon capture. *Energy Environ. Sci.* **2014**, *7*, 4132-4146.

(3) Zhang, Z.; Yao, Z.-Z.; Xiang, S.; Chen, B. Perspective of microporous metal–organic frameworks for CO_2 capture and separation. *Energy Environ. Sci*. **2014**, *7*, 2868-2899.

(4) Lin, X.; Champness, N. R.; Schröder, M. Hydrogen, Methane and Carbon Dioxide Adsorption in Metal-Organic Framework Materials. *Top. Curr. Chem.* **2010**, *293*, 35-76.

(5) Sumida, K.; Rogow, D. L.; Mason, J. A.; McDonald, T. M.; Bloch, E. D.; Herm, Z. R.; Bae, T.-H.; Long, J. R. Carbon Dioxide Capture in Metal–Organic Frameworks. *Chem. Rev.* **2012**, *112*, 724-781.

(6) Andirova, D.; Cogswell, C. F.; Lei, Y.; Choi, S. Effect of the structural constituents of metal organic frameworks on carbon dioxide capture. *Micropor. Mesopor. Mater*. **2016**, *219*, 276-305.

(7) Yu, J.; Xie, L.-H.; Li, J.-R.; Ma, Y.; Seminario, J. M.; Balbuena, P. B. CO_2 Capture and Separations Using MOFs: Computational and Experimental Studies. *Chem. Rev.* **2017**, *117*, 9674-9754.

(8) Li, J.-R.; Ma, Y.; McCarthy, M. C.; Sculley, J.; Yu, J.; Jeong, H.-K.; Balbuena, P. B.; Zhou, H.-C. Carbon dioxide capture–related gas adsorption and separation in metal–organic frameworks. *Coord. Chem. Rev*. **2011**, *255*, 1791-1823.

(9) Liu, J.; Thallapally, P. K.; McGrail, B. P.; Brown, D. R.; Liu, J. Progress in adsorption-based CO_2 capture by metal–organic frameworks. *Chem. Soc. Rev.* **2012**, *41*, 2308-2322.

(10) Belmabkhout, Y.; Guillerm, V.; Eddaoudi, M. Low concentration CO_2 capture using physical adsorbents: Are Metal-Organic Frameworks becoming the new benchmark materials? *Chem. Eng. J.* **2016**, *296*, 386-397.

(11) McDonald, T. M.; Mason, J. A.; Kong, X.; Bloch, E. D.; Gygi, D.; Dani, A.; Crocellà, V.; Giordanino, F.; Odoh, S. O.; Drisdell, W. S.; Vlaisavljevich, B.; Dzubak, A. L.; Poloni, R.; Schnell, S. K.; Planas, N.; Lee, K.; Pascal, T.; Wan, L. F.; Prendergast, D.; Neaton, J. B.; Smit, B.; Kortright, J. B.; Gagliardi, L.;

Bordiga, S.; Reimer, J. A.; Long, J. R. Cooperative insertion of CO_2 in diamine-appended metal-organic frameworks. *Nature* **2015**, *519*, 303-308.

(12) Martínez, F.; Sanz, R.; Orcajo, G.; Briones, D.; Yángüez, V. Amino-impregnated MOF materials for CO_2 capture at post-combustion conditions. *Chem. Eng. Sci.* **2016**, *142*, 55-61.

(13) Li, L.-J.; Liao, P.-Q.; He, C.-T.; Wei, Y.-S.; Zhou, H.-L.; Lin, J.-M.; Lia, X.-Y.; Zhang, J.-P. Grafting alkylamine in UiO-66 by charge-assisted coordination bonds for carbon dioxide capture from high humidity flue gas. *J. Mater. Chem. A* **2015**, *3*, 21849-21855.

(14) Lee, W. R.; Jo, H.; Yang, L.-M.; Lee, H.; Ryu, D. W.; Lim, K. S.; Song, J. H.; Min, D. Y.; Han, S. S.; Seo, J. G.; Park, Y. K.; Moon, D.; Hong, C. S. Exceptional CO_2 working capacity in a heterodiamine-grafted metal–organic framework. *Chem. Sci.* **2015**, *6*, 3697-3705.

(15) Lin, Y.; Kong, C.; Chen, L. Amine-functionalized metal–organic frameworks: structure, synthesis and applications. *RSC Adv.* **2016**, *6*, 32598-32614.

(16) Luo, F.; Yan, C.; Dang, L.; Krishna, R.; Zhou, W.; Wu, H.; Dong, X.; Han, Y.; Hu, T.-L.; O'Keeffe, M.; Wang, L.; Luo, M.; Lin, R.-B.; Chen, B. UTSA-74: A MOF-74 Isomer with Two Accessible Binding Sites per Metal Center for Highly Selective Gas Separation. *J. Am. Chem. Soc*. **2016**, *138*, 5678-5684.

(17) Yan, Y.; Suyetin, M.; Bichoutskaia, E.; Blake, A. J.; Allan, D. R.; Barnett, S. A.; Schröder, M. Modulating the packing of $[Cu_{24}(isophthalate)_{24}]$ cuboctahedra in a triazole-containing metal–organic polyhedral framework. *Chem. Sci.* **2013**, *4*, 1731-1736.

(18) Yazaydin, A. Ö.; Snurr, R. Q.; Park, T.-H.; Koh, K.; Liu, J.; LeVan, M. D.; Benin, A. I.; Jakubczak, P.; Lanuza, M.; Galloway, D. B.; Low, J. J.; Willis, R. R. Screening of Metal−Organic Frameworks for Carbon Dioxide Capture from Flue Gas Using a Combined Experimental and Modeling Approach. *J. Am. Chem. Soc.* **2009**, *131*, 18198-18199.

(19) Alsmail, N. H.; Suyetin, M.; Yan, Y.; Cabot, R.; Krap, C. P.; Lü, J.; Easun, T. L.; Bichoutskaia, E.; Lewis, W.; Blake, A. J.; Schröder, M. Analysis of High and Selective Uptake of CO_2 in an Oxamide-Containing $\{Cu_2(OOCR)_4\}$-Based Metal–Organic Framework. *Chem. Eur. J.* **2014**, *20*, 7317-7324.

(20) Zhou, D.-D.; He, C.-T.; Liao, P.-Q.; Xue, W.; Zhang, W.-X.; Zhou, H.-L.; Zhang, J.-P.; Chen, X.-M. A flexible porous Cu(II) bis-imidazolate framework with ultrahigh concentration of active sites for efficient and recyclable CO_2 capture. *Chem. Commun.* **2013**, *49*, 11728-11730.

(21) Yuan, D.; Zhao, D.; Sun, D.; Zhou, H.-C. An Isoreticular Series of Metal–Organic Frameworks with Dendritic Hexacarboxylate Ligands and Exceptionally High Gas-Uptake Capacity. *Angew. Chem. Int. Ed.* **2010**, *49*, 5357-5361.

(22) Yang, S.; Sun, J.; Ramirez-Cuesta, A. J.; Callear, S. K.; David, W. I. F.; Anderson, D. P.; Newby, R.; Blake, A. J.; Parker, J. E.; Tang, C. C.; Schröder, M. Selectivity and direct visualization of carbon dioxide and sulfur dioxide in a decorated porous host. *Nature Chem*. **2012**, *4*, 887-894.

(23) Plonka, A. M.; Banerjee, D.; Woerner, W. R.; Zhang, Z.; Nijem, N.; Chabal, Y. J.; Li, J.; Parise, J. B. Mechanism of Carbon Dioxide Adsorption in a Highly Selective Coordination Network Supported by Direct Structural Evidence. *Angew. Chem. Int. Ed.* **2013**, *52*, 1692-1695.

(24) Ibarra, I. A.; Mace, A.; Yang, S.; Sun, J.; Lee, S.; Chang, J.-S.; Laaksonen, A.; Schröder, M.; Zou, X. Adsorption Properties of MFM-400 and MFM-401 with CO_2 and Hydrocarbons: Selectivity Derived from Directed Supramolecular Interactions. *Inorg. Chem*. **2016**, *55*, 7219-7228.

(25) Yoon, M.; Moon, D. New Zr (IV) based metal-organic framework comprising a sulfur-containing ligand: Enhancement of CO_2 and H_2 storage capacity. *Micropor. Mesopor. Mater*. **2015**, *215*, 116-122.

(26) Nugent, P.; Belmabkhout, Y.; Burd, S. D.; Cairns, A. J.; Luebke, R.; Forrest, K.; Pham, T.; Ma, S.; Space, B.; Wojtas, L.; Eddaoudi, M.; Zaworotko, M. J. Porous materials with optimal adsorption thermodynamics and kinetics for CO_2 separation. *Nature* **2013**, *495*, 80-84.

(27) Zhai, Q.-G.; Bu, X.; Mao, C.; Zhao, X.; Daemen, L.; Cheng, Y.; Ramirez-Cuesta, A. J.; Feng, P. *Nat. Commun*. **2016**, *7*, 13645.

(28) Prabu, M.; Asha, K. S.; Sinha, M.; Poduval, A.; Mandal, S. The structural diversity, band gap energy and photoluminescence properties of thiophenedicarboxylate based coordination polymers. *CrystEngComm*., **2016**, *18*, 536-543.

(29) Dybtsev, D. N.; Sokolov, I. E.; Peresypkina, E. V.; Fedin, V. P. Design of scaffold-like metal-organic coordination polymers based on dinuclear zinc(II) carboxylate complexes. *Russ. Chem. Bull.* **2007**, *56*, 225-230.

(30) Dybtsev, D. N.; Chun, H.; Kim, K. Rigid and Flexible: A Highly Porous Metal–Organic Framework with Unusual Guest-Dependent Dynamic Behavior. *Angew. Chem. Int. Ed*. **2004**, *43*, 5033-5036.

(31) Kim, Y.; Haldar, R.; Kim, H.; Koo, J.; Kim, K. The guest-dependent thermal response of the flexible MOF $Zn_2(BDC)_2(DABCO)$. *Dalton Trans.* **2016**, *45*, 4187-4192.

(32) Spek, A. L. Structure validation in chemical crystallography. *Acta Crystallogr, Sect. D: Biol. Crystallogr.* **2009**, *65*, 148-155.

(33) Chun, H.; Dybtsev, D. N.; Kim, H.; Kim, K. Synthesis, X-ray Crystal Structures, and Gas Sorption Properties of Pillared Square Grid Nets Based on Paddle-Wheel Motifs: Implications for Hydrogen Storage in Porous Materials. *Chem. Eur. J*. **2005**, *11*, 3521-3529.

(34) Chen, Z.; Xiang, S.; Zhao, D.; Chen, B. Reversible Two-Dimensional−Three Dimensional Framework Transformation within a Prototype Metal−Organic Framework. *Crystal Growth Des.* **2009**, *9*, 5293-5296.

(35) Chen, Z.; Xiang, S.; Arman, H. D.; Li, P.; Zhao, D.; Chen, B. Significantly Enhanced CO_2/CH_4 Separation Selectivity within a 3D Prototype Metal–Organic Framework Functionalized with OH Groups on Pore Surfaces at Room Temperature. *Eur. J. Inorg. Chem*. **2011**, *2011*, 2227-2231.

(36) Burtch, N. C.; Jasuja, H.; Dubbeldam, D.; Walton, K. S. Molecular-level Insight into Unusual Low Pressure CO_2 Affinity in Pillared Metal–Organic Frameworks. *J. Am. Chem. Soc.* **2013**, *135*, 7172-7180.

(37) Mason, J. A.; Sumida, K.; Herm, Z. R.; Krishna, R.; Long, J. R. Evaluating metal–organic frameworks for post-combustion carbon dioxide capture via temperature swing adsorption. *Energy Environ. Sci.* **2011**, *4*, 3030.

(38) Krishna, R. Methodologies for evaluation of metal–organic frameworks in separation applications. *RSC Adv*. **2015**, *5*, 52269-52295.

(39) Myers, A. L.; Prausnitz, J. M. Thermodynamics of mixed-gas adsorption. *AIChE J.* **1965**, *11*, 121-127.

(40) Duan, J.; Higuchi, M.; Krishna, R.; Kiyonaga, T.; Tsutsumi, Y.; Sato, Y.; Kubota, Y.; Takatae, M.; Kitagawa, S. High $CO_2/N_2/O_2$/CO separation in a chemically robust porous coordination polymer with low binding energy. *Chem. Sci.* **2014**, *5*, 660-666.

(41) Torrisi, A.; Bell, R. G.; Mellot-Draznieks, C. Predicting the impact of functionalized ligands on CO_2 adsorption in MOFs: A combined DFT and Grand Canonical Monte Carlo study. *Micropor. Mesopor. Mater.* **2013**, *168*, 225-238.

(42) Torrisi, A.; Mellot-Draznieks, C.; Bell, R. G. Impact of ligands on CO_2 adsorption in metal-organic frameworks: First principles study of the interaction of CO_2 with functionalized benzenes. II. Effect of polar and acidic substituents. *J. Chem. Phys.* **2010**, *132*, 044705.

(43) Besnard, M.; Cabaco, M. I.; Talaga, D.; Danten, Y. Vibrational energy transfer and anisotropy decay in liquid water: Is the Förster model valid? *J. Chem. Phys.* **2008**, *129*, 224511.

Figures and Legends

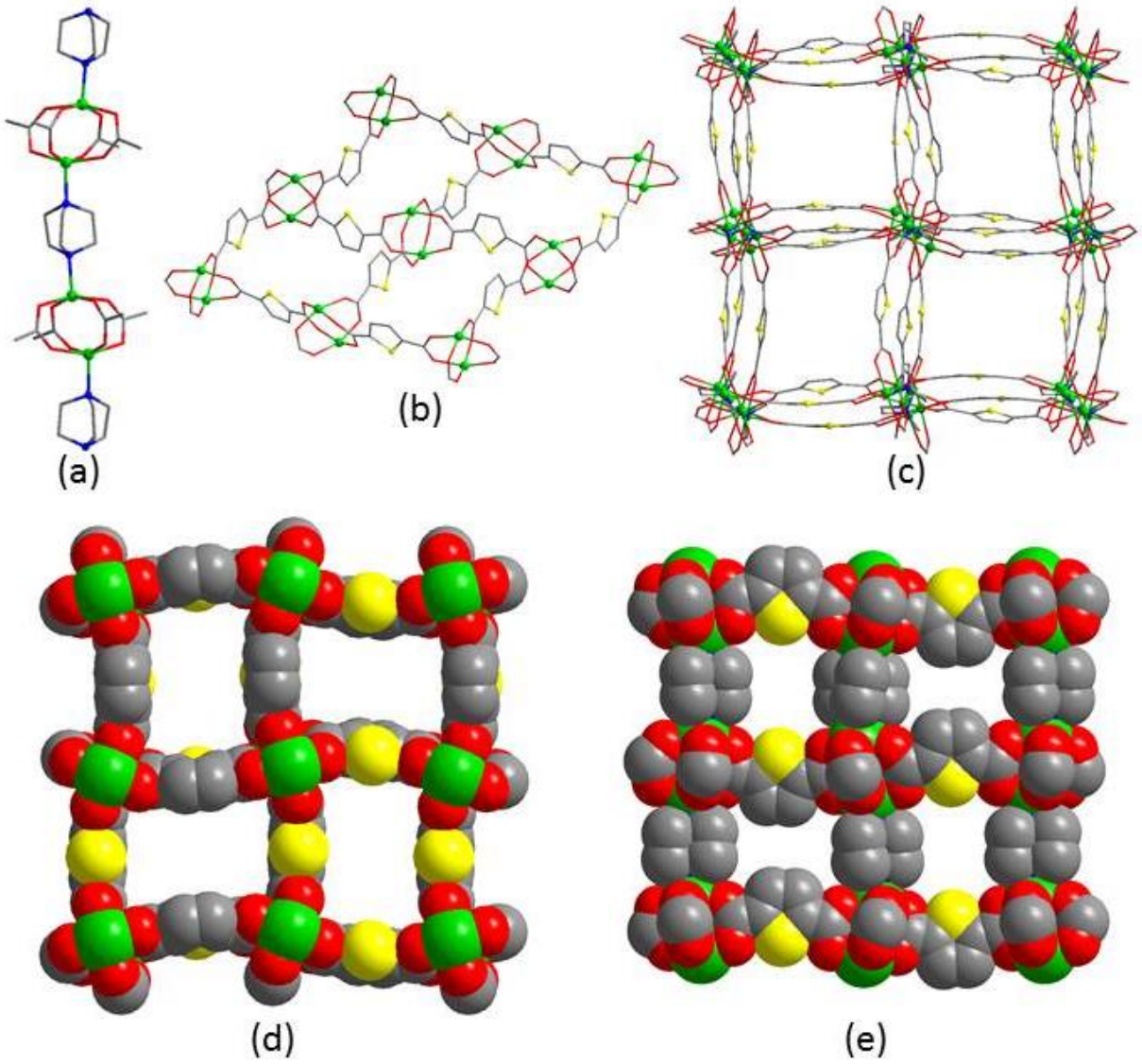

Figure 1. View of the structure of the as-synthesized $[Zn_2(tdc)_2dabco]\cdot 4DMF$ (**1**). The view of the $[Zn_2(OOCR)_4]$ paddle-wheels, connected by dabco ligands (a). The structure of the $[Zn_2(tdc)_2]$ layer (b). Projection of the crystal structure of **1** along the 4-fold axis (c). The aperture of channels along the 4-fold axis (d). The aperture of channels across the 4-fold axis (e). Zn – green, S – yellow, O – red, N – blue, C – grey, hydrogen atoms are not shown.

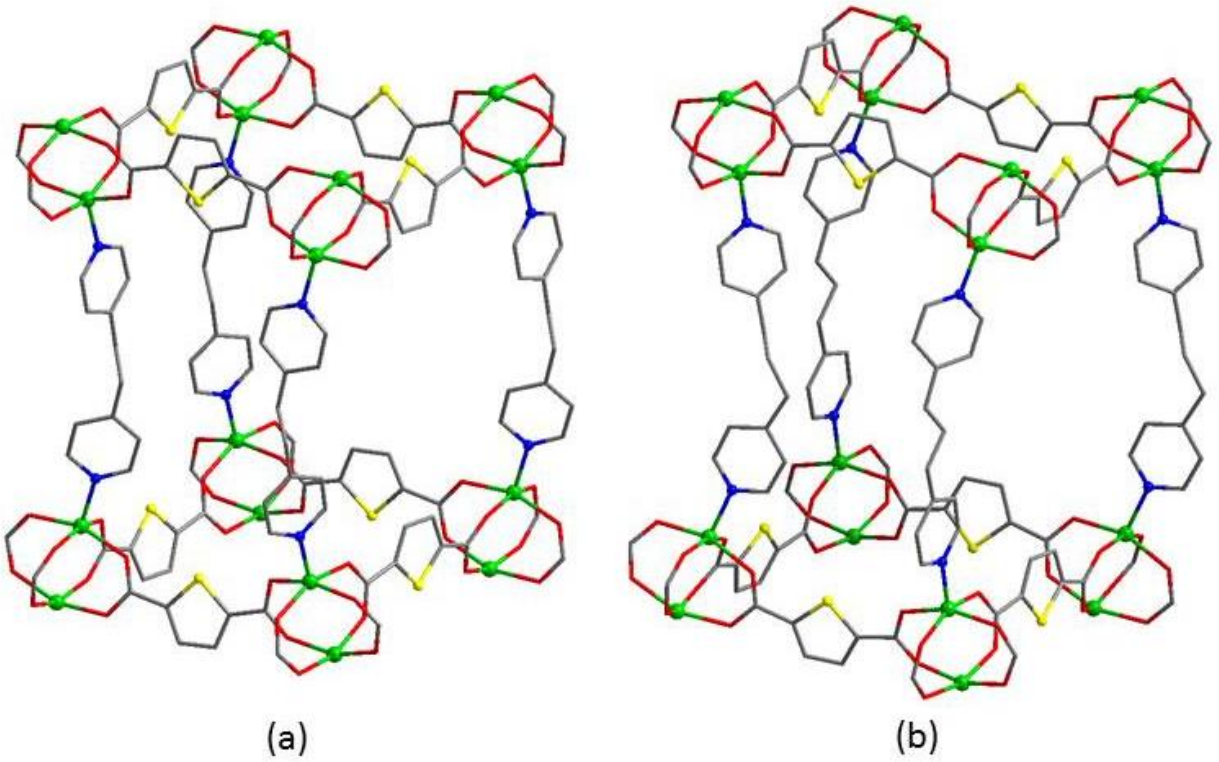

Figure 2. Views of the single nets of $[Zn_2(tdc)_2bpe]\cdot 2DMF$ (**2**)[28] (a) and $[Zn_2(tdc)_2bpp]\cdot 2DMF$ (**3**) (b). Zn – green, S – yellow, O – red, N – blue, C – grey, hydrogen atoms are not shown.

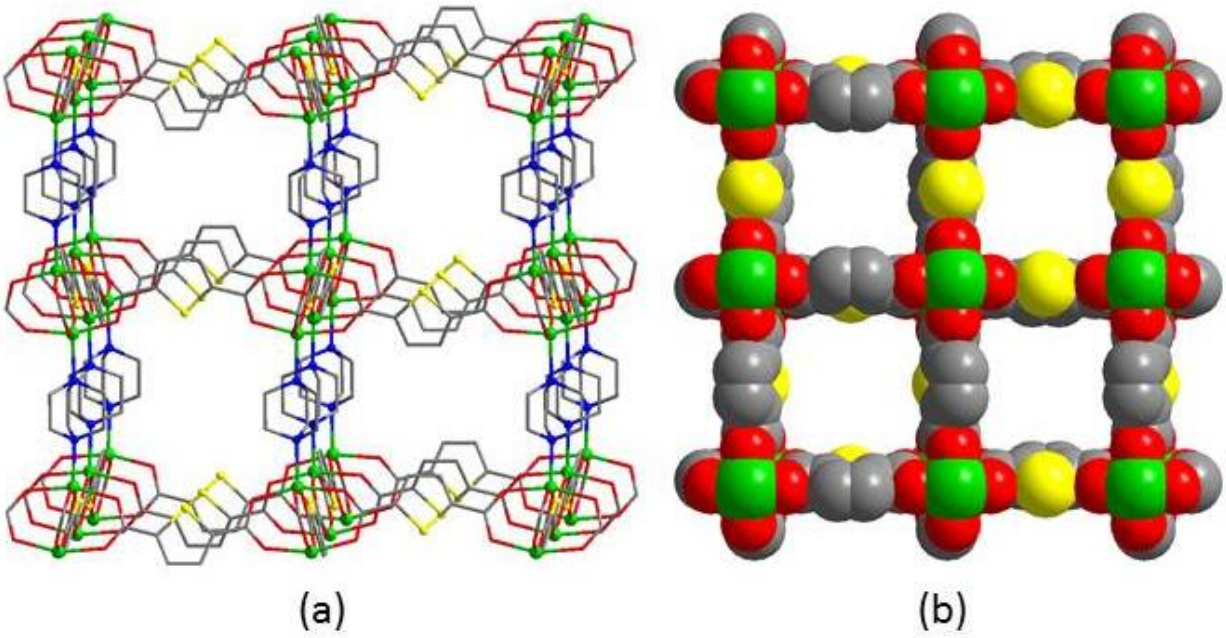

Figure 3. View of the crystal structure of the activated $[Zn_2(tdc)_2dabco]$ (**1a**). Wireframe presentation viewed along the $[Zn_2(tdc)_2]$ layers (a). Van der Waals model view along the 4-fold axis (b). Zn – green, S – yellow, O – red, N – blue, C – grey, hydrogen atoms are not shown.

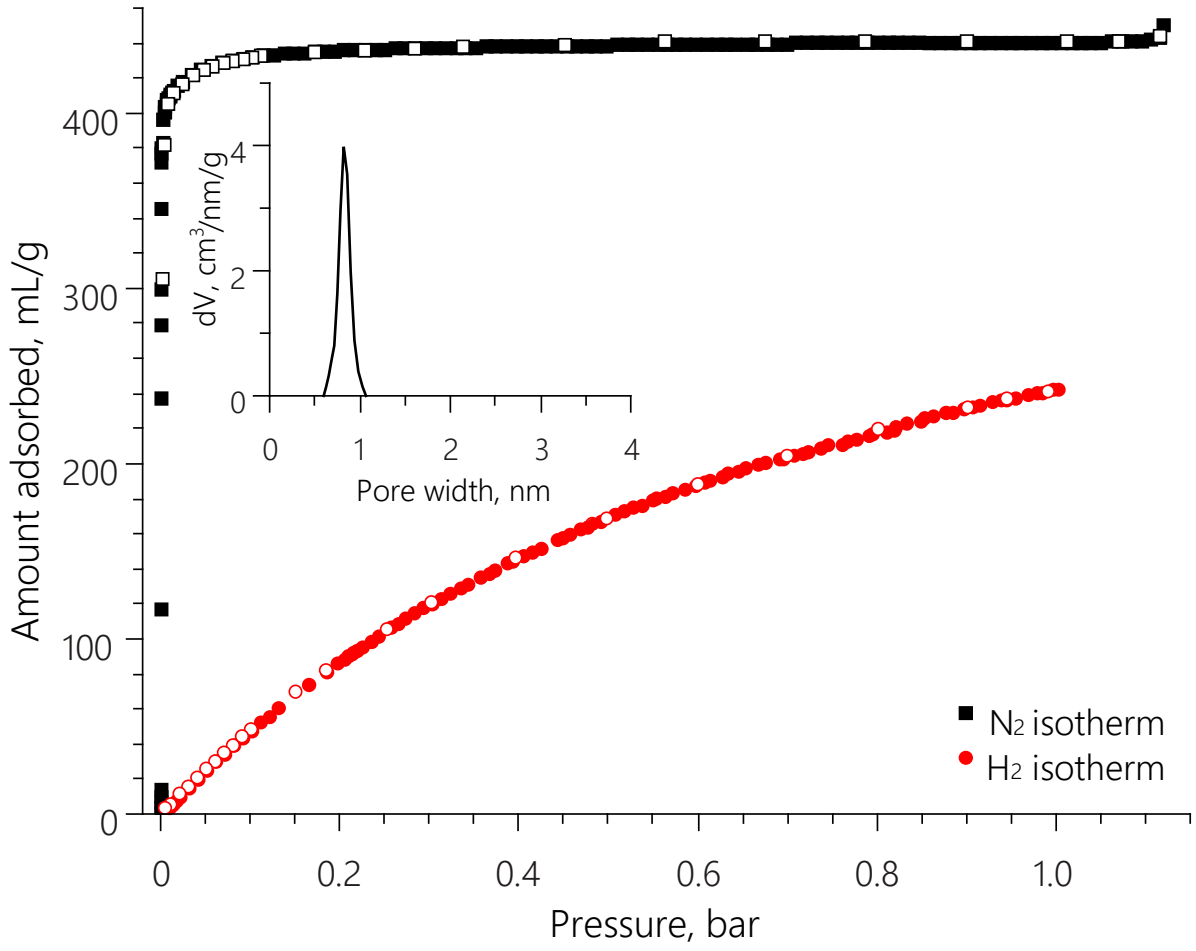

Figure 4. N_2 (black squares) and H_2 (red circles) isotherms for $[Zn_2(tdc)_2dabco]$ (**1a**) at 77K. Adsorption – full symbols, desorption – open symbols. Inset: pore size distribution curve.

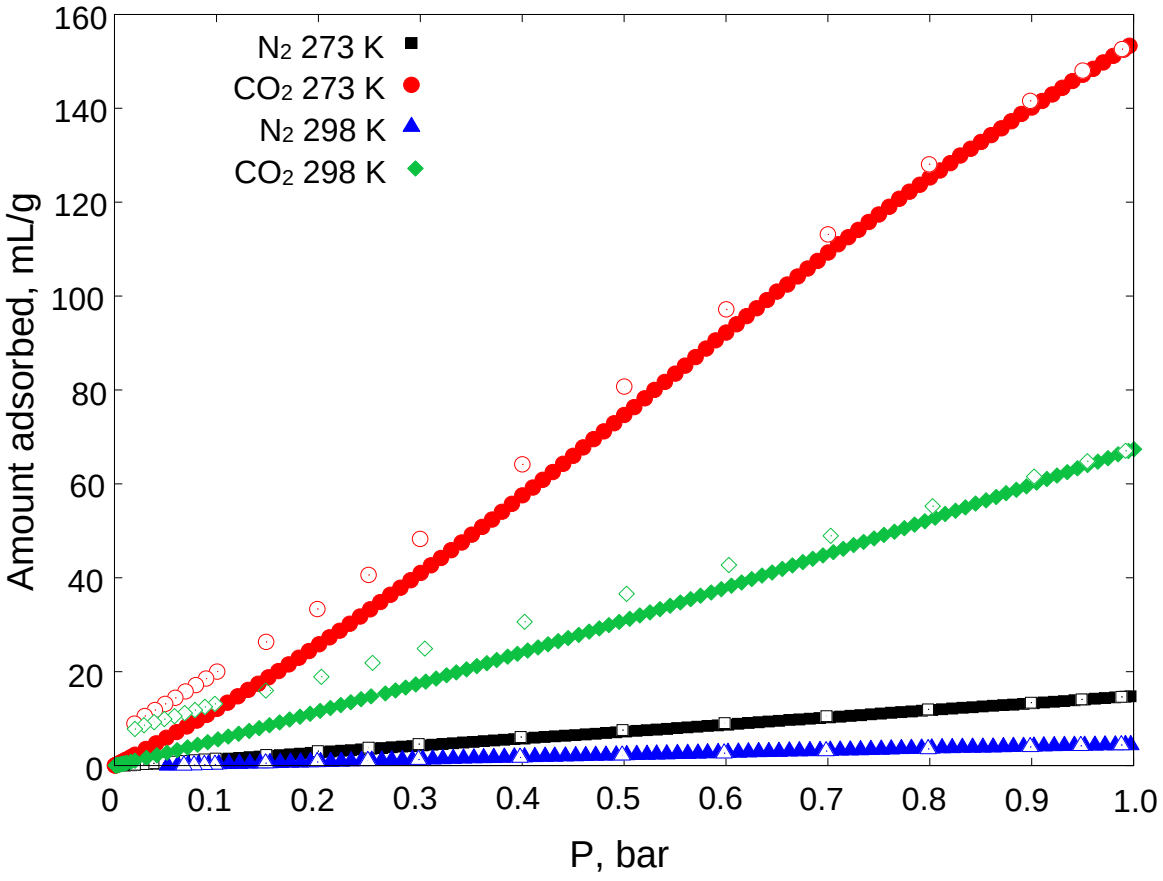

Figure 5. N_2 and CO_2 adsorption (full symbols) and desorption (open symbols) isotherms on $[Zn_2(tdc)_2dabco]$ (**1a**) at 273 K and 298 K.

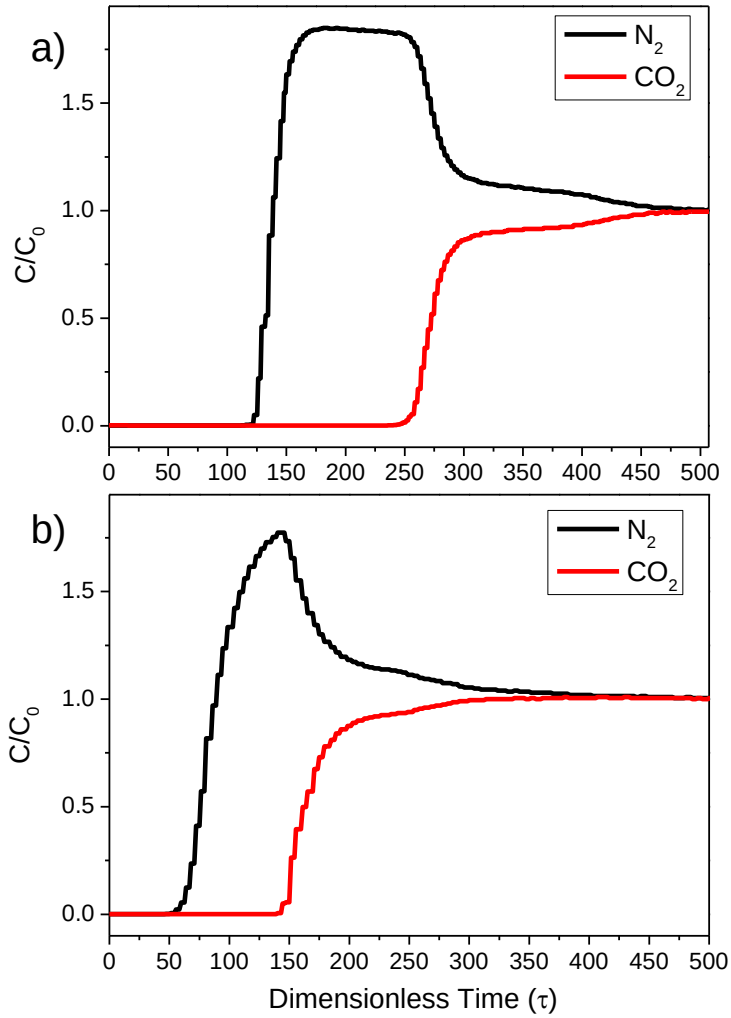

Figure 6. Dimensionless breakthrough curves for N_2/CO_2 mixture (1:1) for **1a** (a) and **4a** (b) at 25 °C and 1 bar.

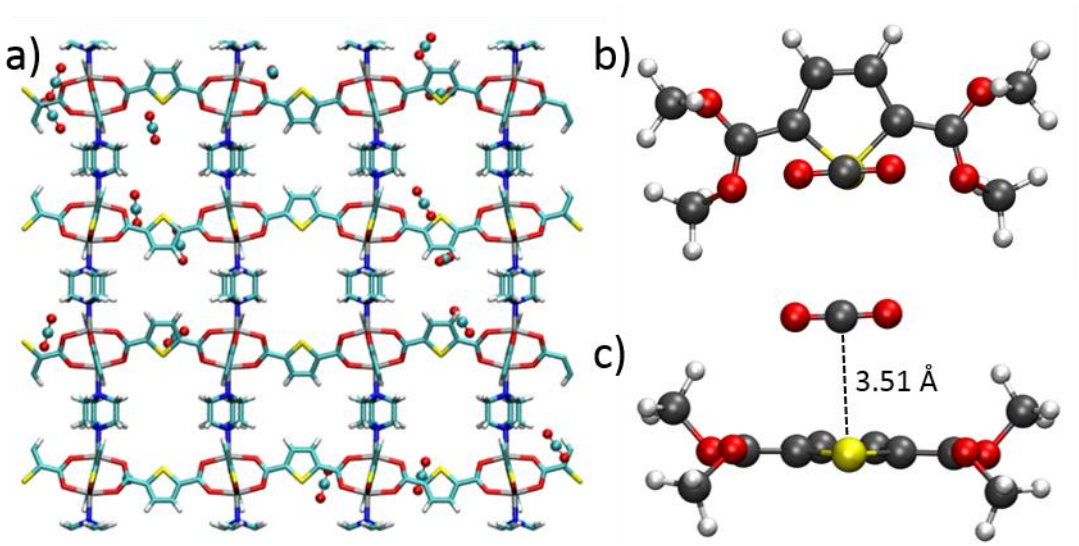

Figure 7. Snapshot from GCMC simulation at low pressure in which the majority of CO_2 molecules were found to be located near to the thiophene ring (a). The DFT-optimized lowest-energy binding site for CO_2 viewed from above the tdc^{2-} fragment (b,c).

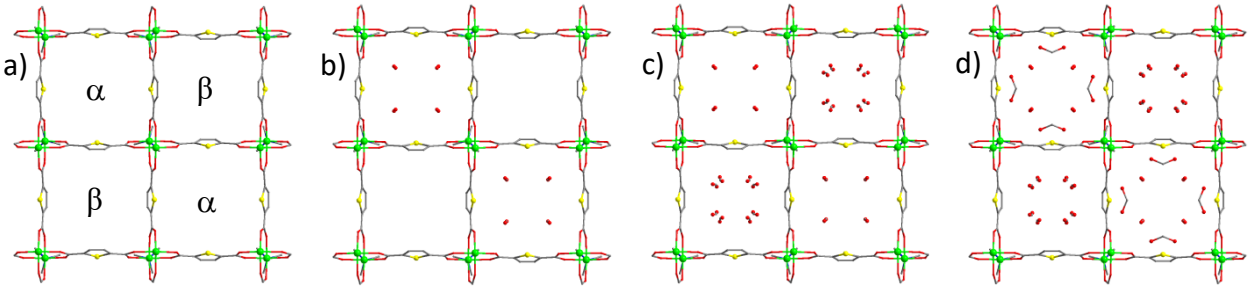

Figure 8. X-ray crystal structures for [Zn_2(tdc)$_2$dabco] (**1a)** as a function of CO_2 loading (projection along the *c* direction). The gas-free activated structure **1a** featuring sulfur-rich (α) and sulfur-poor (β) channels, respectively (a). Views of the binding site for adsorbed CO_2 molecules at gradually increased population of CO_2 in the channels of **1a** (b, c, d).

Table of Contents